# Sulfur Distribution in Bacteriorhodopsin from Multiple Wavelength Anomalous Diffraction Near the Sulfur K-Edge with Synchrotron X-Ray Radiation

Wolfgang Behrens,* Harald Otto,* Heinrich B. Stuhrmann,# and Maarten P. Heyn*
*Biophysics Group, Department of Physics, Freie Universität Berlin, D-14195 Berlin, and #GKSS Forschungszentrum, D-21502 Geesthacht, Germany

ABSTRACT Bacteriorhodopsin contains nine sulfur atoms from the nine methionine residues. The distribution of these sulfur atoms in the projected density map was determined from x-ray diffraction experiments using multiple wavelength anomalous diffraction (MAD) at the sulfur K-edge (5.02 Å) with synchrotron radiation. The experiments were performed with uniaxial samples of oriented purple membranes at room temperature and 86% relative humidity. For such samples only the real part $f'$ (λ) of the resonant scattering amplitude of sulfur contributes to the observed scattering intensity. The sulfur density was determined from the difference in diffraction intensities detected at two wavelengths near the sulfur K-edge that were ~0.004 Å apart. The measured change in $f'$ between these two wavelengths corresponds to 6 electron units. This shows that large anomalous dispersion effects occur near the sulfur K-edge. The in-plane positions of the sulfur atoms of $Met^{32}$, $Met^{56}$, and $Met^{209}$ were determined unambiguously. The difference density from $Met^{20}$, $Met^{60}$, $Met^{118}$, and $Met^{145}$ is concentrated in the interior of the seven $\alpha$-helical bundle, overlaps strongly in the projected density map, and cannot be resolved at the resolution of these experiments (8.2 Å). This method of localizing individual sulfur atoms can be applied to other two-dimensional protein crystals and is promising in conjunction with the site-directed introduction of sulfur atoms by the use of cysteine mutants.

## INTRODUCTION

Anomalous dispersion is a powerful method for determining biological structures, particularly since the advent of tunable synchrotron x-ray sources (Rosenbaum et al., 1971; Helliwell, 1992; Hendrickson, 1991; Fourme and Hendrickson, 1990). For technical reasons these applications have been limited so far to the wavelength region around 1 Å, where the x-ray absorption is low and experiments can be performed with diffractometers in air. Sulfur and phosphorus are atoms of high biological interest. Unfortunately, because of their low $Z$ values, the K-edges of S and P are at 5.02 Å and 5.78 Å respectively, i.e., in a wavelength region with very high absorption, requiring sample and detectors to be in high vacuum. At 5.0 Å, the penetration depth of X-rays in air is only 3 cm. To avoid these absorption problems, methionine was replaced in a number of cases by selenomethionine, thereby shifting the K-edge down to 0.98 Å, into the accessible x-ray region (Yang et al., 1990; Hendrickson et al., 1990). Multiple wavelength anomalous diffraction (MAD) with selenomethionine has become a routine method in protein crystallography. However, it is obviously an advantage to be able to work with naturally occurring sulfur without having to replace it with Se. Moreover, in the case of phosphorus this strategy does not work, because no biologically active replacement for this element is available.

The use of anomalous dispersion of sulfur for the structure determination of proteins was proposed by Herzenberg and Lau (1967). These authors suggested the use of molybdenum L radiation to cover the anomalous region near the sulfur K-edge. Hendrickson and Teeter (1981) used the anomalous dispersion of sulfur to solve the structure of the small protein crambin (46 residues, 6 sulfur atoms). For this purpose they used the single wavelength of Ni-filtered Cu-K$\alpha$ radiation (1.54 Å), which is far removed from the absorption edge of sulfur (5.02 Å). The weak residual anomalous scattering effect of S at 1.54 Å ($f' = 0.33$e and $f'' = 0.56$e) was sufficient to determine the phases down to 1.5 Å in this unusual case.

In this study we have determined the sulfur distribution, projected onto the membrane plane, of the membrane protein bacteriorhodopsin (bR), using multiple wavelength anomalous diffraction (MAD) at the sulfur K-edge. This protein contains nine methionine residues with one sulfur atom each, three bond lengths removed from the $\alpha$-carbon of the backbone. BR has no cysteine residues. The positions of the nine methionine residues in the sequence are indicated in Fig. 1. Within the membrane, the bR molecules are arranged in a two-dimensional hexagonal lattice of $P_3$ symmetry. The unit cell dimension is 62 Å. The structure of bR was studied by cryoelectron microscopy (Henderson et al., 1990; Grigorieff et al., 1996) and by neutron diffraction (Seiff et al., 1985; Heyn et al., 1989; Hauss et al., 1990), using these natural two-dimensional lattices. A refined model with an in-plane resolution of 3.5 Å is available (Grigorieff et al., 1996). Recently, after submission of our manuscript, a 2.5-Å resolution structure was obtained by x-ray diffraction with three-dimensional microcrystals (Pebay-Peyroula et al., 1997).

*Received for publication 11 August 1997 and in final form 6 April 1998.*
Address reprint requests to Dr. Maarten P. Heyn, Department of Physics, Freie Universität Berlin, Arnimallee 14, D-14195 Berlin, Germany. Tel.: 49-30-838-6174; Fax: 49-30-838-5186; E-mail: heyn@physik.fu-berlin.de.

0006-3495/98/07/255/09 $2.00

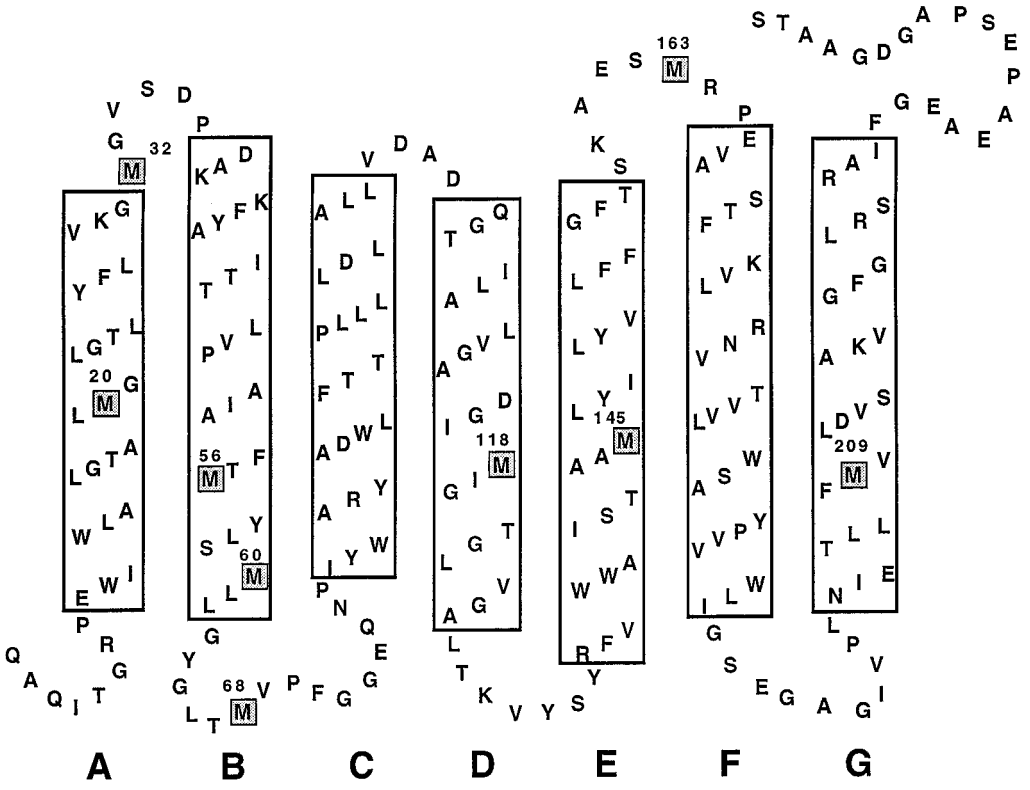


FIGURE 1 Primary and secondary structures of bacteriorhodopsin. Boxed regions labeled A to G correspond to the seven transmembrane $\alpha$-helices. The nine sulfur-containing methionine residues are highlighted and are marked by their residue numbers.

Our diffraction experiments at the sulfur K-edge were performed with hydrated oriented purple membrane films. The diffraction pattern of these uniaxial powder samples is of the Debye-Scherrer type. The $(h, k)$ and $(-h, -k)$ reflections occur at the same scattering angle and therefore cannot be distinguished. The contribution of anomalous scattering to the intensity is in this case proportional to $f'(\lambda)$, the real part of the sulfur resonant scattering amplitude. Our experiments were therefore performed at two wavelengths, $\lambda_1$ and $\lambda_2$, near the K-edge, which were chosen in such a way that the difference in the dispersion, $\Delta f' = f'(\lambda_2) - f'(\lambda_1)$, was at maximum and the difference in absorption $\Delta f''$ was close to zero. The intensity differences, $I(\lambda_1) - I(\lambda_2)$, were then used together with the phase information available from cryoelectron microscopy to determine the sulfur positions by Fourier difference methods. In this way the positions of the sulfur atoms of $Met^{32}$, $Met^{56}$, and $Met^{209}$ could be identified directly in the projected density map. The results are in excellent agreement with the model from cryoelectron microscopy (Grigorieff et al., 1996). The density peaks of the sulfur atoms of the remaining six methionines overlap strongly in the interior of the seven $\alpha$-helical bundle and cannot be resolved at the limited resolution (8.2 Å) of our experiment. The calculated density for these six sulfur atoms is also in good agreement with the latest available model structure (Grigorieff et al., 1996).

A major advantage of the MAD method, as applied here to determine the location of single atoms, is that the differences in scattered intensities are induced by changing the wavelength by less than 0.01 Å, so that only one sample is required. In this way scaling problems are avoided. In experiments in which single amino acids were localized by heavy atom labeling (Krebs et al., 1993; Behrens, 1995; Behrens et al., manuscript submitted for publication), two samples, a derivatized and an underivatized one, were needed. With uniaxial two-dimensional membrane crystals it is virtually impossible to produce identical samples.

Our results show that MAD experiments, performed with sulfur-containing proteins at 5.02 Å, are feasible and that valuable structural information can be gained in this way. The three sulfur positions in the side chains of $Met^{32}$, $Met^{56}$, and $Met^{209}$ were not previously determined in a direct way.

Additional sulfur atoms can be introduced into a protein by site-directed mutagenesis with cysteine mutants. The combination of anomalous dispersion at the sulfur K-edge with cysteine mutants seems to be particularly promising for the investigation of structural aspects of membrane proteins for which often only two-dimensional crystals are available. Moreover, this method may also be applied to the solution of the structure of proteins by the use of three-dimensional crystals. As a regular constituent of proteins, sulfur can serve as a native anomalous scatterer. Promising results of

single crystal diffraction at the sulfur K-edge were recently reported for trypsin (Stuhrmann et al., 1997).

## MATERIALS AND METHODS

### Sample preparation

Purple membranes from *Halobacterium salinarium* were prepared by standard procedures. Concentrated purple membrane suspension (0.5 mg) in deionized water was applied to a piece of 4-$\mu$m Trespaphan foil (Hoechst, Germany). This drop was allowed to dry for 24 h at 86% relative humidity in a closed box in the presence of a saturated KCl solution. The resulting hydrated oriented films covered an area of $\sim 4 \times 10$ mm$^2$ and had a thickness of $\sim 50$ $\mu$m. In the presence of absorption, the optimal thickness for scattering is given by $1/\mu(\lambda)$, where $\mu(\lambda)$ is the absorption coefficient of the sample at the wavelength $\lambda$. Because of the strong absorption around 5 Å, the optimal thickness of the sample is $\sim 50$ $\mu$m. Trespaphan was chosen because at this energy, the scattering from the foil itself provided only a homogeneous background. Other support materials, such as mylar, show distinct reflections (data not shown) that are difficult to separate from the diffraction of the sample. Polyethylene foils are known to have Debye-Scherrer diffraction rings that are caused by the stretching of the films during production (Brown, 1949).

Within the purple membrane, the bR molecules are arranged in a hexagonal lattice of $P_3$ symmetry with unit cell dimension $d = 62.4$ Å (Glaeser et al., 1985). In a film, the purple membranes are stacked on top of each other in a random way, leading to a uniaxial sample with the average membrane normal perpendicular to the plane of the supporting foil. The resulting diffraction pattern is thus of the Debye-Scherrer type.

### Sample holder

As shown in Fig. 2, the foil with the purple membrane film is separated from a second 4-$\mu$m Trespaphan film by an O-ring. A piece of moist tissue paper inside this volume prevents dehydration of the sample. This sandwich assembly is pressed together in a vacuum-tight way between a conical stainless steel cover plate and an aluminum sample holder plate by four screws (see Fig. 2). The support plate is mounted on a goniometer and can be rotated and moved laterally inside the vacuum chamber by stepping motors. At the highest x-ray intensities employed in these experiments at 5 Å, the first signs of radiation damage (bleaching of the sample) were already apparent after 20 min at room temperature. The problem of radiation damage has been discussed (Henderson, 1990).

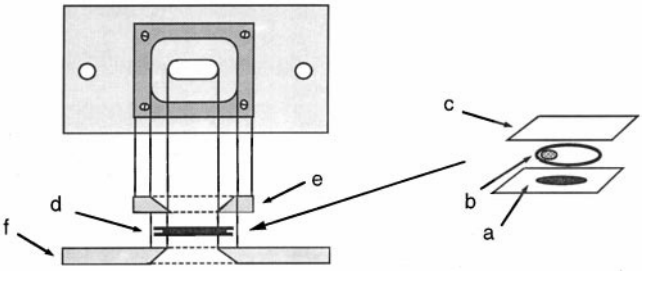


FIGURE 2 Expanded view of sample holder. The purple membrane film is on the top of the 4-$\mu$m Trespaphan foil (*a*) and is surrounded by an O-ring (*b*). The sample volume is closed off by a second piece of Trespaphan foil on top (*c*). Inside this volume there is a small piece of moist tissue paper to prevent dehydration. This sandwich assembly (*d*) is clamped by four screws between a conical stainless steel cover ring (*e*) and an aluminum sample holder plate (*f*).

### Synchrotron beamline and dedicated soft x-ray diffractometer

The experiments were performed at beamline A1 of HASYLAB at DESY (Hamburg, Germany). This beamline, originating in a bending magnet, was designed for small-angle x-ray scattering at wavelengths up to 6.9 Å and has been described in detail (Stuhrmann et al., 1991). The relevant features of the set-up will be described here only briefly. The monochromator consists of a combination of two mirrors and a single crystal. A gold-coated toroidal mirror and a planar quartz mirror serve as premonochromators and help suppress higher harmonics from the Ge(111) single crystal monochromator. No contamination by third-order harmonics was detected. The resolution of the monochromator $\Delta\lambda/\lambda$ was $3.2 \times 10^{-4}$. Because a single monochromator was used, the crystal and the diffractometer assembly (all in high vacuum) have to be moved in a ($\theta$, $2\theta$) fashion as the wavelength is varied (Fig. 3). These ($\theta$, $2\theta$) scans are performed with high accuracy by appropriate stepping motors. To reduce the intensity loss due to the very high x-ray absorption around 5 Å, the number of windows was minimized and the complete scattering experiment was performed in a vacuum. Two slits were mounted after the monochromator and in front of the sample with areas of $4 \times 4$ and $2 \times 4$ mm$^2$, respectively. The first one reduced the scattering background from the monochromator.

The diffraction pattern is detected by four two-dimensional detectors as described elsewhere (Gabriel, 1977; Boulin et al., 1988). These four multiwire proportional detectors have an area of $300 \times 300$ mm$^2$ each and are depicted in Fig. 3. The detector (labeled CD) that detects the scattering in the forward direction is called the central detector. To avoid problems when the diffraction data from several detectors are merged, the scattered x-rays were detected only by the central detector (see Fig. 3). This was achieved by choosing an appropriate sample-to-detector distance.

The intensity of the primary beam was monitored by two ionization chambers ($I_1$, $I_2$; see Fig. 3). The first one ($I_1$) is situated between the monochromator and the sample. The second one ($I_2$) is part of the beam stop. The ratio of the ionization chamber signals, $I_1/I_2$, was used to calculate extended x-ray absorption fine structure (EXAFS) spectra. Data collection and stepping motors were controlled from a VAX 750.

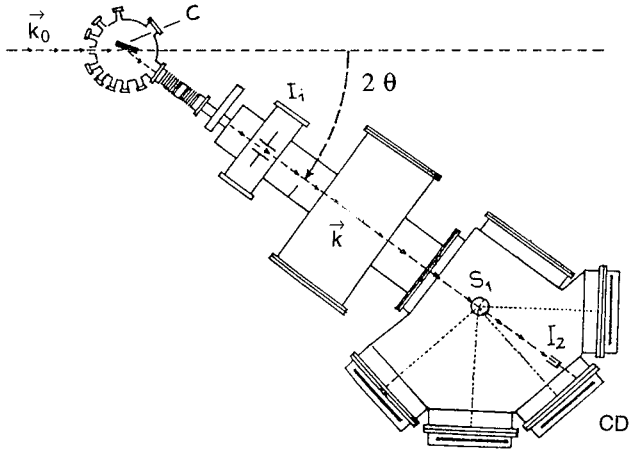


FIGURE 3 The soft x-ray diffractometer at beamline A1 of HASYLAB. The premonochromatized beam transmitted by the focusing double-mirror system (not shown) is reflected by the single crystal C. The wavelength $\lambda$ is varied by rotating the crystal and the evacuated camera by $\theta$ and $2\theta$, respectively, around the common axis. The angles $\theta$ and $2\theta$ are changed in steps of 0.8 arcseconds and 1.6 arcseconds, respectively, which is better than required by the energy resolution of the monochromator system. The beam intensity is monitored by the ionization chambers $I_1$ and $I_2$. The central detector used in these experiments is labeled CD.

## Data collection

A sulfur powder sample was used to find the K-edge ($E$ = 2471 eV, $\lambda$ = 5.018 Å) from its EXAFS spectrum. The purple membrane sample was then mounted and its sulfur K-edge found by using the EXAFS spectrum. For the uniaxial purple membrane sample with $P_3$ symmetry, the reflections occur at

$$|\vec{s}(h, k)| = \frac{2 \sin \theta}{\lambda} = \frac{2}{d\sqrt{3}} \sqrt{h^2 + hk + k^2} \qquad (1)$$

The $(h, k)$ and $(-h, -k)$ reflections thus appear on the same ring, and the observed intensity is $\overline{I(h, k)} = \frac{1}{2}[I(h, k) + I(-h, -k)]$.

The structure factor $F(h, k)$ for the two-dimensional lattice is the sum of the contributions from the sulfur atoms $F_L$(label) and from the rest of the protein $F_p$:

$$F(h, k) = F_p(h, k) + F_L(h, k) \qquad (2)$$

The contribution from the nonresonant part of the sulfur atomic scattering factor is included in $F_p$. Because all chemically equivalent sulfur atoms have the same resonant atomic scattering factor $f = f' + if''$, $F_L$ is given by the product

$$F_L = (f' + if'')\tilde{F}_L \qquad (3)$$

$\tilde{F}_L$ is the sum of the phase factors for the sulfur positions. The intensity $I(h, k)$ is thus given by

$$I(h, k) = |F_p|^2 + 2f'|F_p| \cdot |\tilde{F}_L| \cdot \cos(\varphi_p - \varphi_L) + 2f''|F_p| \cdot |\tilde{F}_L| \cdot \sin(\varphi_p - \varphi_L) + (f'^2 + f''^2) \cdot |\tilde{F}_L|^2 \qquad (4)$$

$\varphi_p$ and $\varphi_L$ are the phases of $F_p$ and $\tilde{F}_L$, respectively. In going from $(h, k)$ to $(-h, -k)$, the phases $\varphi_p$ and $\varphi_L$ change sign. In the observed intensity $\bar{I}$, the average of $I(h, k)$ and $I(-h, -k)$, the sine term therefore cancels:

$$\overline{I(h, k)} = |F_p|^2 + 2f'|F_p| \cdot |\tilde{F}_L| \cdot \cos(\varphi_p - \varphi_L) + (f'^2 + f''^2) \cdot |\tilde{F}_L|^2 \qquad (5)$$

Finally, it can easily be shown that with only nine sulfur atoms in bacteriorhodopsin, the quadratic term in $|f|^2$ can be neglected compared to the linear interference term. Thus only the real part $f'$ contributes to $\bar{I}$:

$$\overline{I(h, k, \lambda)} = |F_p|^2 + 2f'|F_p| \cdot |\tilde{F}_L| \cdot \cos(\varphi_p - \varphi_L) \qquad (6)$$

Only $f'(\lambda)$ changes when the wavelength is varied infinitesimally by 0.004 Å near the K-edge. The largest change in $\overline{I(h, k)}$ with wavelength is thus expected between the two wavelengths $\lambda_1$ and $\lambda_2$ with the largest $\Delta f' = f'(\lambda_1) - f'(\lambda_2)$. To find these optimal wavelengths, $f''(\lambda)$ was obtained from the EXAFS spectrum. The corresponding dispersion $f'(\lambda)$ was then calculated from $f''(\lambda)$ by Kramers-Kronig transformation. The best choice of $\lambda_1$ and $\lambda_2$ was then determined from the $f'(\lambda)$ spectrum (see Results). A x-ray absorption near edge structure (XANES) spectrum was used to locate $\lambda_1$ and $\lambda_2$ accurately. Diffraction patterns of the sample were taken at the two wavelengths following the sequence $(\lambda_1, \lambda_2, \lambda_2, \lambda_1)_n$. At each wavelength, a diffraction pattern was collected for 5 or 10 min. In this way, pairs of diffraction patterns at $\lambda_1$ and $\lambda_2$ were obtained under conditions that were as close as possible. This procedure minimizes systematic errors, such as drift in beam position or wavelength, and the unavoidable continuous decrease in intensity (storage time ~6 h). The detector response was measured using the isotropic x-ray fluorescence from a powder sample of sulfur or dithiothreitol.

## Data analysis

The two-dimensional diffraction patterns were first corrected for the detector response. Because the normal to the central detector makes an angle of 11° with the incident beam, the circular Debye-Scherrer rings are deformed into ellipses on the detector. The detected intensity of the isotropic fluorescence radiation varies with the scattering angle. The detector response was corrected for this effect. The optimal midpoint and axial ratio for each ellipse were determined by least-squares curve fitting. The diffraction intensities were then integrated over a 60° sector of the ellipse. This procedure was carried out for each 10-min diffraction pattern separately to correct for small changes in beam direction. A background subtraction was performed for every one-dimensional integrated diffraction pattern. The spectra were then normalized by the x-ray intensity. The intensities for each $(\lambda_1, \lambda_2)$ pair were then subtracted. The diffraction peaks for the shorter wavelength occur at slightly larger Bragg angles than for the longer wavelength. Although the energy difference $\Delta E$ is only ~2 eV (at $E$ = 2470 eV, i.e., ~0.1%), this effect is clearly observable and has to be corrected. Without this correction, the intensity difference for a single reflection has the shape of the derivative of the line. A scaling factor for the $s$ axis of the diffraction pattern at one wavelength was chosen such that the derivative features in the difference intensities disappeared. This happened when the centers of each of the Gaussian peaks in both spectra occurred at the same $s$ value. This is a very sensitive and effective correction procedure. The strong and nonoverlapping (1,1) and (2,0) reflections and the (4,3) reflection were used for this purpose. Scaling factors on the order of 0.994 were required. Part of the data analysis was performed with the program MADMAN (Huetsch and Kuehnholz, unpublished results).

Twelve difference pairs $I(\lambda_1) - I(\lambda_2)$ were collected and corrected in this way. After all corrections, the data were pooled into one difference spectrum. A Fourier difference map for the sulfur distribution was then obtained from these intensity differences in the usual way, using as coefficients

$$\overline{|F(h, k, \lambda_1)|} - \overline{|F(h, k, \lambda_2)|} \approx \frac{\overline{I(h, k, \lambda_1)} - \overline{I(h, k, \lambda_2)}}{2\sqrt{\overline{I(h, k, \lambda_1)}}} \qquad (7)$$

The phase information and splitting factors were taken over from cryo-electron microscopy as described (Plöhn and Büldt, 1986; Krebs et al., 1993). It has been shown experimentally that this procedure is justified and works very well in the case of bacteriorhodopsin (Seiff et al., 1985; Koch et al., 1991).

## RESULTS

The XANES spectrum of a purple membrane sample near the K-edge of sulfur (data not shown) was converted into a $f''(\lambda)$ spectrum using the optical theorem. The $f''(\lambda)$ data were put on an absolute scale of electron equivalents by scaling to 0.5 on the low energy side, using the tabulated values (Cromer and Liberman, 1970). Two absorption peaks that are ~10 eV apart are resolved in the $f''$ spectrum of Fig. 4 (*top*). Purple membranes contain 10 lipid molecules per bacteriorhodopsin molecule. Of these lipids, ~30% are glycosulfolipids with sulfate headgroups (Kates et al., 1982). XANES measurements on methionine and ammonium sulfate showed that the sulfur absorption edges occurred at 2471 and 2480 eV, respectively (Munk, 1988). Based on these results, the K-edge of 2471 eV can be assigned to the divalent sulfur of the methionines and the K-edge at 2480 eV to the hexavalent sulfur of the glycosulfolipids. The real part $f'(\lambda)$ of the sulfur anomalous scattering amplitude,

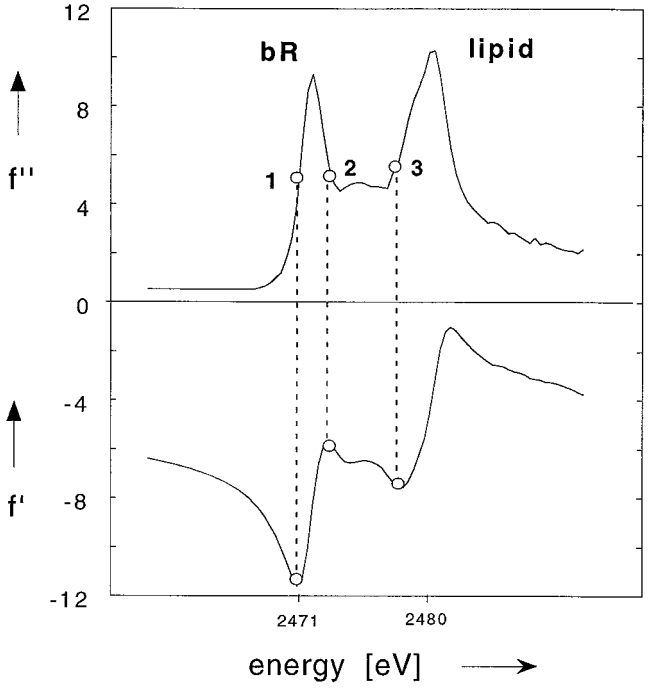


FIGURE 4 Real and imaginary parts of the resonant x-ray scattering amplitude of purple membranes near the sulfur K-edge. A XANES spectrum was first measured and corrected for $\lambda^3$ background. At 100 energy points the absorption was measured for 1 s. In going from one energy point to the next, the monochromator stepping motor moved 50 steps. $f''(\lambda)$ was obtained from the XANES spectrum and put on an absolute scale, using the tabulated values on the low energy side (Cromer and Liberman, 1970). The two edges labeled 1 and 3 (at 2471 and 2480 eV) are due to the divalent sulfur of the methionines of bR and the hexavalent sulfur of the glycosulfolipids, respectively. $f'(\lambda)$ was obtained from $f''(\lambda)$ by Kramers-Kronig transformation. The vertical scale is expressed in electron equivalents. The largest change in $f'$ for the divalent sulfur occurs between the energies labeled 1 and 2.

obtained from $f''(\lambda)$ by Kramers-Kronig transformation, is presented in the lower panel of Fig. 4. It is apparent from Fig. 4 that the energies marked by $E_1$ and $E_2$ are optimal for the anomalous dispersion experiment on methionine, because the change in $f'$ between these points is largest, close to 6 electron equivalents. At the same time, the absorption $f''$ is almost the same at these energies, so that no absorption corrections are required. The energy difference between points one and two is ~2 eV, corresponding to a wavelength difference of ~0.004 Å. The diffraction patterns at $\lambda_1$ and $\lambda_2$ were measured and corrected as described in Materials and Methods. Fig. 5 shows the integrated one-dimensional diffraction patterns at $\lambda_1$ (*dashed line*) and $\lambda_2$ (*solid line*) after 10 min of data collection at each wavelength. These data form one ($\lambda_1$, $\lambda_2$) pair. The data are corrected for detector response and background. The reflections from the hexagonal lattice are labeled by the Miller indices (*h, k*) below each peak. The diffraction pattern at $\lambda_1$ (*dashed line*) is shifted to the right, so that intensity differences can be recognized more easily. Major intensity differences occur for the (1, 1), (4, 0), and (4, 3) reflections. Smaller intensity differences can be clearly discerned for the (2, 0), (2, 2), and (4, 1) reflections. Both positive and negative changes occur. The (6, 1) reflection was the highest order observed and corresponds to a resolution of 8.24 Å. In Fig. 6 the intensity difference patterns for all 12 ($\lambda_1$, $\lambda_2$) pairs are pooled. The vertical scale is in counts and provides a measure of the statistics. These intensity differences were then used as described in Materials and Methods to calculate the Fourier difference map for the methionine sulfur density. In Fig. 7 the sulfur density is shown in the hexagonal unit cell, which contains three bR molecules. The density is presented, using equidistant contour lines ranging from 22% to 89% of the positive difference density. Five distinct regions of the density are marked *a*–*e*. The outer boundary of the bR density is outlined by two low-density contour lines (2% and 7% of the positive density). The approximate positions of the seven $\alpha$-helices are marked A–G. From the structural model of bR, it is known that four of the methionine side chains point to the interior of the $\alpha$-helical bundle (Henderson et al., 1990). The sulfur atoms of these methionines ($Met^{20}$, $Met^{60}$, $Met^{118}$, and $Met^{145}$) contribute to the two interior maxima (*d*) and (*e*) and cannot be resolved at our limited resolution (8.2 Å). To help in the assignment of the three isolated density regions *a*, *b*, and *c*, the positions of the nine methionine sulfur atoms from the refined cryoelectron microscopy model (Grigorieff et al., 1996) are indicated in Fig. 7. The residue numbers are shown in Fig. 8. The seven sulfur atoms from methionines with well-defined positions in $\alpha$-helices are marked by a black dot, and the two sulfurs from the methionines in the BC and EF loops are marked by a cross (see also Fig. 1). These longer loops are mobile and/or disordered (Behrens et al., manuscript submitted for publication; Grigorieff et al., 1996), so that the density from these atoms is possibly smeared out (see Discussion). The seven positions (*filled circles*) with low temperature factors in the refined model (Grigorieff et al., 1996) fit quite well with the S distribution obtained. From a comparison between Figs. 7 and 8, the isolated density regions *a*, *b*, and *c* can be clearly identified with the sulfur atoms of $Met^{32}$ (helix A), $Met^{56}$ (helix B), and $Met^{209}$ (helix G). For these three sulfur atoms we obtain in-plane coordinates of (0.081, −0.356), (0.103, −0.100), and (0.406, −0.031), respectively. The positions are expressed here in reduced coordinates, with the origin and *x*, *y* directions as indicated in Fig. 7. The two sulfurs from $Met^{20}$ and $Met^{60}$ apparently contribute to the density region *d* of Fig. 7, which has about twice the density of the isolated regions *a* and *b*. Residues $Met^{118}$ and $Met^{145}$ contribute likewise to the density region *e* of Fig. 7, which has again about twice the density of one of the three isolated sulfur atoms. The positions of the sulfur atoms of $Met^{68}$ and $Met^{163}$ (⊗) are uncertain, because these residues are in loops for which little or no density was observed (Behrens et al., manuscript submitted for publication; Grigorieff et al., 1996) with very high temperature factors (Grigorieff et al., 1996).

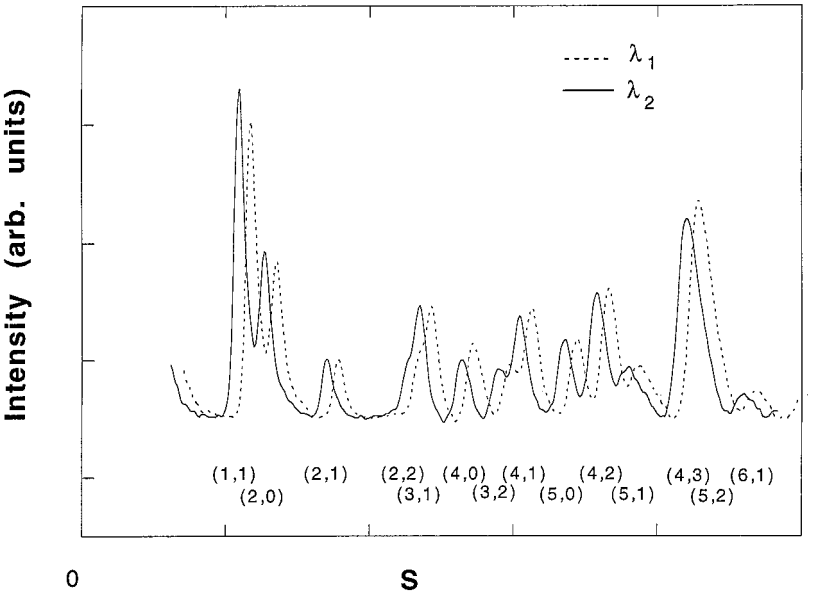


FIGURE 5 Diffraction patterns of the same purple membrane sample at the wavelengths corresponding to point 1 (– – –) and point 2 (——) of Fig. 4. Each data set was collected in 10 min. The two-dimensional diffraction pattern was integrated and corrected as described in Materials and Methods. For a better presentation, the pattern at $\lambda_1$ is displaced slightly to the right.

## DISCUSSION

We have used multiple wavelength anomalous diffraction (MAD) at the sulfur K-edge (5.018 Å) to determine the in-plane positions of the nine sulfur atoms in bacteriorhodopsin. The technical problems associated with these experiments, which are mainly due to the very high absorption at this wavelength, were solved by minimizing the number of windows in the beam line. At the medium resolution of our experiments (8.2 Å), the in-plane positions of the three sulfur atoms of $Met^{32}$, $Met^{56}$, and $Met^{209}$ could be determined directly for the first time. The four side chains of $Met^{20}$, $Met^{60}$, $Met^{118}$, and $Met^{145}$ point to the interior of the $\alpha$-helical bundle. Their sulfur densities overlap and cannot be resolved at this resolution in the in-plane density map. $Met^{32}$ is in the short AB loop near the end of helix A. Residues $Met^{68}$ and $Met^{163}$ are in the middle of the two long loops connecting helices BC and EF, respectively. For these loops only weak density was observed, and the temperature factors of ~350 $Å^2$ were very high (Grigorieff et al., 1996). This suggests that these residues are part of a highly disordered or mobile loop domain. This is in agreement with a recent determination of the position of residue 160 in the EF loop by site-directed heavy-atom labeling (Behrens et al., manuscript submitted for publication). These authors observed no extra density for the mutant A160 C labeled with mercury. It is thus quite likely that, because of the dynamic and/or static disorder of these longer loops, the contributions of $Met^{68}$ and $Met^{163}$ (*crosses* in Fig. 7) to the sulfur map are smeared out. The structure of the BC loop, which includes $Met^{68}$, was stated to be quite uncertain ("essentially a guess"; Grigorieff et al., 1996) and is possibly incorrect, because no density was observed near this region in Fig. 7. After submission of this manuscript, a three-dimensional structure at a resolution of 2.5 Å was published (Pebay-

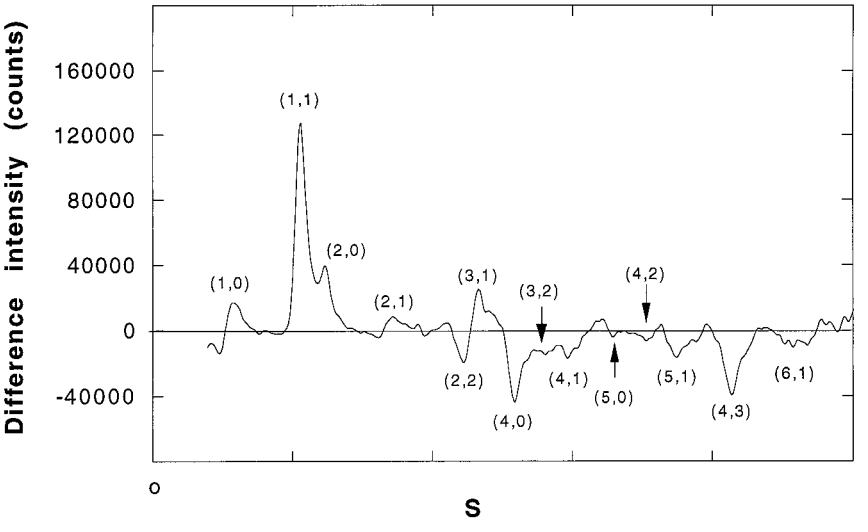


FIGURE 6 Pooled difference intensities $I(\lambda_1) - I(\lambda_2)$ from 12 ($\lambda_1$, $\lambda_2$) pairs.

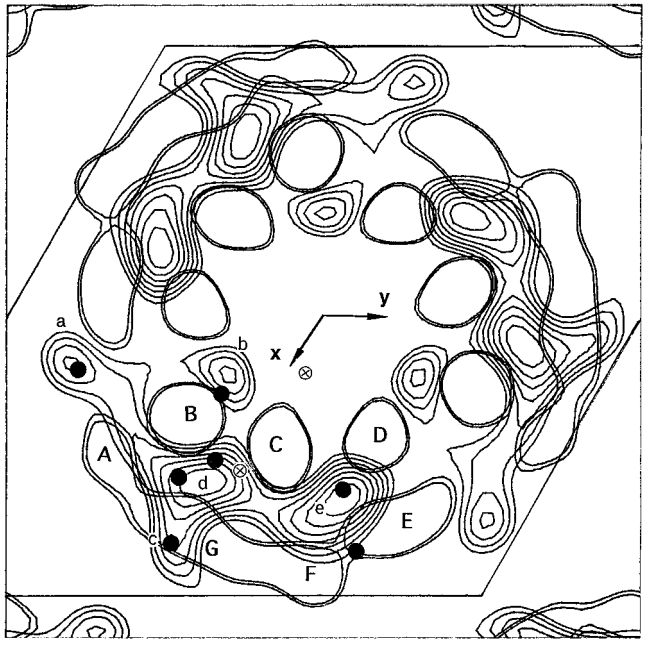


FIGURE 7 Fourier difference map for the sulfur density of bacteriorhodopsin. The isolated density maxima, corresponding to single sulfur atoms, are labeled *a*, *b*, and *c*. *d* and *e* are density maxima to which several methionines contribute. The outer boundary of the bR density is indicated by two contour lines. The approximate positions of the seven $\alpha$-helices are indicated by A–G. There are three bR molecules per unit cell. The origin and directions of the oblique (*x*, *y*) coordinates are as indicated. The positions of the nine methionine sulfur atoms obtained by cryoelectronmicroscopy (Grigorieff et al., 1996) are marked by ● (the seven sulfur atoms in $\alpha$-helices), or by ⊗ (the two sulfur atoms in loops).

Peyroula et al., 1997). The atomic coordinates are not yet available from the Brookhaven Data Bank, so that a direct comparison of the sulfur positions is not possible. Comparison with the structural model of Grigorieff et al. (1996), however, showed a "high degree of similarity in the helical regions" (Pebay-Peyroula et al., 1997), so that no significant changes are expected in the positions of the methionines in the transmembrane part of the structure. This leaves the loop methionines. No density was observed for residues 157–166 of the EF loop (Pebay-Peyroula et al., 1997), in agreement with our argument and observation (Behrens et al., manuscript submitted for publication) that $Met^{163}$ is in a highly disordered domain. However, for the AB and BC loops, ordered structures were obtained that differ substantially from those obtained by cryoelectron microscopy (Grigorieff et al., 1996). In particular, the structure of the BC loop is completely different. It is thus indeed quite likely that the position of $Met^{68}$ (*cross* in Fig. 7 outside the sulfur density) is incorrect.

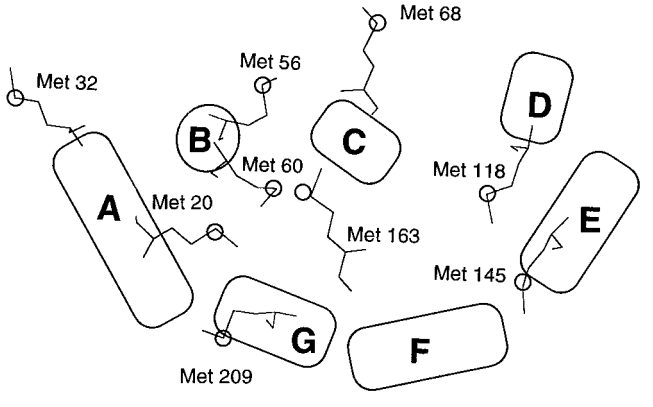


FIGURE 8 Side chains and in-plane positions of the sulfur atoms (○) of the nine methionines taken from the refined structural model of Grigorieff et al. (1996). The seven helices are marked A–G. Their form indicates the direction and extent of helix tilt.

In previous MAD work with purple membranes at the sulfur K-edge (Munk, 1988), anomalous dispersion data were collected out to the (4, 1) reflection, corresponding to a resolution of 11.8 Å. At this lower resolution, only the two larger density maxima labeled *d* and *e* in Fig. 7 could be discerned, in good agreement with our results. The data of Fig. 6 show that strong anomalous dispersion effects occur in the higher order (5, 1), (4, 3), and (5, 2) reflections, which make major contributions to the higher resolution density map of Fig. 7.

The experiment described here shows that anomalous dispersion of sulfur at the K-edge can be used for structure determination. The strong absorption of matter at this energy poses a major problem. Technical improvements can help overcome this and other problems and help make such experiments more practicable. Of utmost importance for these MAD experiments is high wavelength stability and sufficient intensity to detect the small intensity differences. Third-generation synchrotron radiation sources provide conditions of beam stability and intensity that are significantly better than available in our experiments at HASYLAB. In particular, the use of wigglers or undulators, as opposed to the bending magnets used here, will improve the brilliance by two orders of magnitude. The higher intensity at 5 Å will allow the use of two-crystal monochromators, rather than the single-crystal monochromator used here. Cooling of the crystals will further reduce the wavelength instability. The higher intensity will also allow the use of monochromators of higher resolution. In our experiments a Ge (111) crystal was used. This choice was dictated by the very high reflecting power of this crystal, which was of critical importance because of the low beam intensity. A serious disadvantage of the Ge (111) crystal, however, is its low resolution $\Delta\lambda/\lambda$ of only $3.2 \times 10^{-4}$. This is only 2.5 times smaller than the difference between the wavelengths $\lambda_1$ and $\lambda_2$ used in our experiments. A significant gain in the anomalous dispersion signal may thus be expected with improved resolution by a better monochromator. With higher beam intensities, this could be achieved by using crystals of lower reflecting power, such as Si (111) or Si (220), which have much better resolutions of $1.4 \times 10^{-4}$ and $6.0 \times 10^{-5}$ respectively (Matsushita and Hashizume, 1983). Of these two possibilities, the Si (111) reflection would be usable at the high wavelength of 5 Å. The radiation damage could be reduced by cooling the sample inside

the high vacuum system. This would help to improve the signal in particular for the higher order reflections. The detection system used here (multiwire proportional counters) can be further optimized. The detection efficiency and the lateral resolution can be improved by an appropriate choice of the gas mixture and an increase in the gas pressure, respectively. Image plates and CCD detectors are also sensitive to soft x-rays and may lead to better detection systems. Implementation of these technical improvements will make MAD measurements at the sulfur K-edge more practicable in the near future.

One advantage of this MAD method is that only one sample is required. In this way, scaling problems can be avoided that occur when data sets from labeled and unlabeled samples are used. A further advantage is isomorphism. Heavy atom labels may introduce a perturbation in the structure of the protein, particularly when an internal site is selected. MAD with naturally occurring sulfur circumvents this problem. There is perfect isomorphism because the same crystal is used at several wavelengths. A third advantage is the small amount of sample required for these experiments. Here we used 0.5 mg of protein. With even less material (e.g., 0.2 mg), diffraction data of sufficient quality could be collected (Behrens, unpublished results). This is of interest for the class of receptor proteins in which usually only very small amounts of purified crystalline material are available.

In this section we discuss the limitations of the method used in this paper. An intrinsic limitation is the long wavelength of ~5 Å. This has the following consequences: 1) The resolution is at best 2.5 Å. 2) With $\sin\theta$ proportional to $\lambda$, expensive detector systems with very large solid angle are required. 3) The very small penetration depth of ~30 $\mu$m in the condensed phase leads to radiation damage and large temperature gradients in the sample. The experiments require high spatial stability of the x-ray beam, which is only realized at some synchrotrons. The method as presented here requires that a low-resolution structure already be available. Phase information and splitting factors for reflections that overlap in the powder pattern were taken from cryoelectron microscopy. Given such data, additional structural information on the position of the sulfur atoms is obtained from the observed MAD intensity differences. Fortunately, a considerable number of low-resolution protein structures are known from cryoelectron microscopy with 2D protein lattices (Kühlbrandt, 1992; Jap et al., 1992), so this requirement does not pose a limitation on future applications. We point out that it is possible to obtain the required phase information from the MAD data of a powder pattern (Prandl, 1990).

The method of MAD at the sulfur K-edge with uniaxial membrane powder samples apparently works, because the results are in excellent agreement with the model from cryoelectron microscopy (Grigorieff et al., 1996). It requires a two-dimensional crystalline protein lattice for which a low-resolution structure should be available from cryoelectron microscopy. A large number of such systems exist; these are discussed in two review articles (Jap et al., 1992; Kühlbrandt, 1992). Many of these systems consist of membrane proteins. It is very difficult to produce three-dimensional crystals of membrane proteins, and most of them are too large to be solved by high-resolution NMR in solubilized form. Cryoelectron microscopy with two-dimensional protein crystals is thus often the only method for obtaining structural information for membrane proteins. Such two-dimensional crystals are ideally suited for the method described in this paper. Among the receptor proteins, rhodopsin is a promising example for future applications. For this protein, 2D crystals and low-resolution structures (6–8 Å) are available from squid, frog, and cattle (Davies et al., 1996; Schertler and Hargrave, 1995; Schertler et al., 1993). Additional sulfur can be introduced at well-defined positions in the structure by site-directed mutagenesis. Likewise, it is possible to delete sulfur. We have recently demonstrated the feasibility of this approach by replacing the amino acid glutamine at position 105 in the CD loop of bacteriorhodopsin with cysteine, and determining the position of the extra sulfur atom by the methods described in this paper. This promising result was reported in a preliminary communication (Behrens et al., 1997).

We thank Dr. Barbara Munk and Dr. Matthias Huetsch for their help in the early stages of this project.

This research was supported by grant 03-HE4-FUB3 from the Bundesministerium für Bildung und Forschung (MPH).

## REFERENCES

Behrens, W. 1995. Neue methodische Ansätze zur Strukturuntersuchung der Loops des Membranproteins Bacteriorhodopsin. Röntgendiffraktion mit ortsspezifisch gebundenen Schweratomen und anomaler Dispersion an der Schwefel K-Kante. Ph.D. thesis. Freie Universität Berlin.

Behrens, W., H. Otto, R. Mollaaghababa, U. Alexiev, H. G. Khorana, and M. P. Heyn. 1997. X-ray diffraction studies on bacteriorhodopsin: localization of loop- and sulfur-containing residues. *Biophys. J.* 72:A208.

Boulin, C. J., R. Kempf, A. Gabriel, and M. H. J. Koch. 1988. Data acquisition systems for linear and area x-ray detectors using delay line readout. *Nucl. Instrum. Methods.* A269:312–320.

Brown, A. 1949. X-ray diffraction studies of the stretching and relaxing of polyethylene. *J. Appl. Phys.* 20:552–558.

Cromer, D. T., and D. Liberman. 1970. Relativistic calculation of anomalous scattering factors for x-rays. Report LA-4403, Los Alamos Scientific Laboratory, Los Alamos, NM.

Davies, A., G. F. X. Schertler, B. E. Gowen, and H. R. Saibil. 1996. Projection structure of an invertebrate rhodopsin. *J. Struct. Biol.* 117: 36–44.

Fourme, R., and W. A. Hendrickson. 1990. Analysis of macromolecular structures by the method of multiwavelength anomalous diffraction. *In* Synchrotron Radiation and Biophysics. S. S. Hasnain, editor. Harwood Publishers, Chichester. 156–175.

Gabriel, A. 1977. Position sensitive x-ray detector. *Rev. Sci. Instrum.* 48:1303–1305.

Glaeser, R. M., J. S. Jubb, and R. Henderson. 1985. Structural comparison of native and deoxycholate treated purple membrane. *Biophys. J.* 48: 775–780.

Grigorieff, N., T. A. Ceska, K. H. Downing, J. M. Baldwin, and R. Henderson. 1996. Electron-crystallographic refinement of the structure of bacteriorhodopsin. *J. Mol. Biol.* 259:393–421.

Hauss, T., S. Grzesiek, H. Otto, J. Westerhausen, and M. P. Heyn. 1990. Transmembrane location of retinal in bacteriorhodopsin by neutron diffraction. *Biochemistry.* 29:4904–4913.

Helliwell, J. R. 1992. Macromolecular Crystallography with Synchrotron Radiation. Cambridge University Press, Cambridge.

Henderson, R. 1990. Cryo-protection of protein crystals against radiation damage in electron and x-ray diffraction. *Proc. R. Soc. Lond. Biol.* 241:6–8.

Henderson, R., J. M. Baldwin, T. A. Ceska, F. Zemlin, E. Beckmann, and K. H. Downing. 1990. Model for the structure of bacteriorhodopsin based on high-resolution electron cryo-microscopy. *J. Mol. Biol.* 213: 899–929.

Hendrickson, W. A. 1991. Determination of macromolecular structures from anomalous diffraction of synchrotron radiation. *Science.* 254: 51–58.

Hendrickson, W. A., J. R. Horton, and D. M. Le Master. 1990. Selenomethionyl proteins produced for analysis by multiwavelength anomalous diffraction (MAD): a vehicle for direct determination of three-dimensional structure. *EMBO J.* 9:1665–1672.

Hendrickson, W. A., and M. M. Teeter. 1981. Structure of the hydrophobic protein crambin determined directly from the anomalous scattering of sulphur. *Nature.* 290:107–113.

Herzenberg, A., and H. S. M. Lau. 1967. Anomalous scattering and the phase problem. *Acta Crystallogr.* 22:24–28.

Heyn, M. P., J. Westerhausen, I. Wallat, and F. Seiff. 1989. High sensitivity neutron diffraction of membranes: location of the Schiff base end of the chromophore of bacteriorhodopsin. *Proc. Natl. Acad. Sci. USA.* 85:2146–2150.

Jap, B. K., M. Zulauf, T. Scheybani, A. Hefti, W. Baumeister, U. Aebi, and A. Engel. 1992. 2D crystallization: from art to science. *Ultramicroscopy.* 46:45–84.

Kates, M., S. C. Kushwaha, and G. D. Sprott. 1982. Lipids of purple membrane from extreme halophiles and of methanogenic bacteria. *Methods Enzymol.* 80:98–111.

Koch, M. H. J., N. A. Dencher, D. Oesterhelt, H.-J. Plöhn, G. Rapp, and G. Büldt. 1991. Time-resolved x-ray diffraction study of structural changes associated with the photocycle of bacteriorhodopsin. *EMBO J.* 10: 521–526.

Krebs, M. P., W. Behrens, R. Mollaaghababa, H. G. Khorana, and M. P. Heyn. 1993. X-ray diffraction of a cysteine-containing bacteriorhodopsin mutant and its mercury derivative. Localization of an amino acid residue in the loop of an integral membrane protein. *Biochemistry.* 32:12830–12834.

Kühlbrandt, W. 1992. Two-dimensional crystallization of membrane proteins. *Q. Rev. Biophys.* 25:1–49.

Matsushita, T., and H. Hashizume. 1983. X-ray monochromators. *In* Handbook on Synchrotron Radiation, Vol. 1A. E. E. Koch, editor. North-Holland, Amsterdam. 261–314.

Munk, B. 1988. Strukturuntersuchungen an dem Membranprotein Bakteriorhodopsin mit Hilfe der anomalen Röntgenstreuung an der K-Absorptionskante des Schwefels. Ph.D. thesis. University of Hamburg.

Pebay-Peyroula, E., G. Rummel, J. P. Rosenbusch, and E. M. Landau. 1997. X-ray structure of bacteriorhodopsin at 2.5 Å from microcrystals grown in lipidic cubic phases. *Science.* 277:1676–1681.

Plöhn, H.-J., and G. Büldt. 1986. The determination of label positions in membrane proteins by neutron and anomalous x-ray diffraction of powder samples. *J. Appl. Crystalogr.* 19:255–261.

Prandl, W. 1990. Phase determination and Patterson maps from multiwavelength powder data. *Acta Crystallogr. A.* 46:988–992.

Rosenbaum, G., K. C. Holmes, and J. Witz. 1971. Synchrotron radiation as a source for x-ray diffraction. *Nature.* 230:434–437.

Schertler, G. F. X., and P. A. Hargrave. 1995. Projection structure of frog rhodopsin in two crystal forms. *Proc. Natl. Acad. Sci. USA.* 92: 11578–11582.

Schertler, G. F. X., C. Villa, and R. Henderson. 1993. Projection structure of rhodopsin. *Nature.* 362:770–772.

Seiff, F., I. Wallat, P. Ermann, and M. P. Heyn. 1985. A neutron diffraction study on the location of the polyene chain of retinal in bacteriorhodopsin. *Proc. Natl. Acad. Sci. USA.* 82:3227–3231.

Stuhrmann, S., K. S. Bartels, W. Braunwarth, R. Doose, F. Dauvergne, A. Gabriel, A. Knöchel, M. Marmotti, H. B. Stuhrmann, C. Trame, and M. S. Lehmann. 1997. Anomalous dispersion with edges in the soft x-ray region: first results of diffraction from single crystals of trypsin near the K-edge of sulfur. *J. Synchrotron Radiat.* 4:298–310.

Stuhrmann, H. B., G. Goerigk, and B. Munk. 1991. Anomalous x-ray scattering. *In* Handbook on Synchrotron Radiation, Vol. 4. M. Koch and E. Rubenstein, editors. Elsevier Science Publishers, Amsterdam. 555–580.

Yang, W., W. A. Hendrickson, R. J. Crouch, and Y. Satow. 1990. Structure of ribonuclease H phased at 2 Å resolution by MAD analysis of the selenomethionyl protein. *Science.* 249:1398–1405.